Multifunctionality of Layered Materials

Septiany, Liany

DOI:
10.33612/diss.182500502

Chapter 2

Experimental Techniques

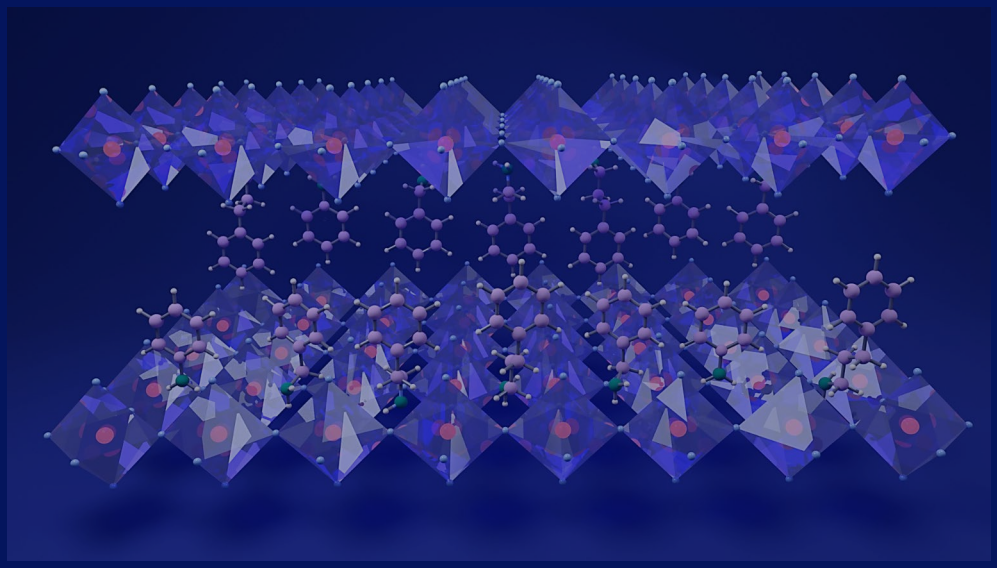

2.1 Synthesis

2.1.1 Solid-state Reaction

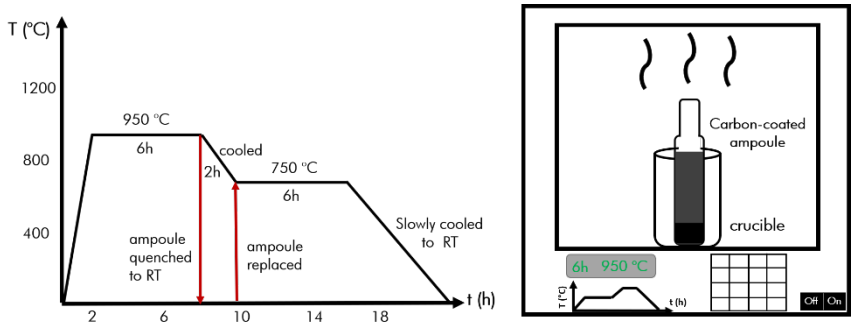

Figure 2.1 *Temperature profile of the furnace and solid-state reaction for preparation of* $(GeSe)_{1-x}(AgBiTe_2)_x$ *thermoelectric materials*

Polycrystalline samples of the thermoelectric materials $(GeSe)_{1-x}(AgBiTe_2)_x$ with x = 0, 0.05, 0.1, 0.15, 0.2 and 0.3 were synthesized by a solid-state reaction method. High purity powders of the elements Ge, Se, Ag, Bi, and Te stored in a nitrogen-filled glove box were weighed according to the stoichiometric ratio for each composition and transferred to a ball-mill machine for high-energy milling at 250 rpm for 12 hours. The mixed powder was then loaded into a commercially obtained carbon-coated quartz ampoule. Carbon-coated tubes were used to prevent reaction between the precursors and the tube walls, which can lead to non-stoichiometric products. In addition, to prevent oxidation of the elements during the synthesis, the ampoule was vacuum sealed using a flame. The ampoule was then placed inside a box furnace in a vertical position and heated to the liquid phase to ensure homogenous mixing of the elements. The heating procedure is presented in Fig. 2.1; after holding at 950 °C the ampoule was quenched to room temperature. The empty furnace was cooled down to 750 °C, and the ampoule was then placed back in the furnace, annealed for 6h and then slowly cooled to room temperature. After many attempts it was found that this heating procedure was necessary to obtain the desired phase. The products were obtained in the form of ingots, which were removed after breaking the ampoule. Parts of the ingots were hand-ground to a powder for X-ray diffraction measurement, and other parts were cut into rectangular shapes and polished for thermoelectric property measurements.

2.1.2 Single-Crystal Synthesis of Layered Hybrid Perovskites

Single-crystals of all the layered organic-inorganic perovskite compounds studied in this thesis were grown using one of the two methods described below. In both cases, the relevant transition metal halide salt was used as the inorganic precursor. The organic precursor used was either the relevant amine (in liquid form) or the amine mixed with HCl to obtain the respective organoammonium salt.

In the latter case, the amine was mixed with HCl in the molar ratio of 1:1 in ethanol solvent. The reaction mixture was left to dry overnight on a hot plate. The resulting salts were then washed several times with diethyl ether to ensure that all excess precursors were removed. The powder was placed in a vacuum oven to evaporate all solvent and any remaining water.

2.1.2.1 Slow-Evaporation Method

The single crystals of manganese-based layered perovskites studied in this thesis were obtained by the simple slow-evaporation method. The synthesis scheme is given in Fig. 2.2.

The organic and inorganic components were dissolved in separate Erlenmeyer flasks using ethanol as the solvent. The contents of the two flasks were then combined and stirred for ~2h. The solution was divided into different flasks and placed inside a 60 °C oven. After approximately one week, single crystals had grown inside the flask and were harvested for various measurements.

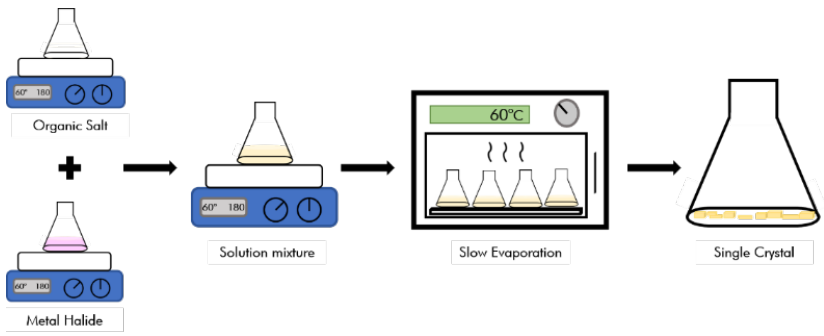

Figure 2.2 *Slow-evaporation method for preparation of Mn-based layered hybrid perovskites*

2.1.2.2 Anti-Solvent Method

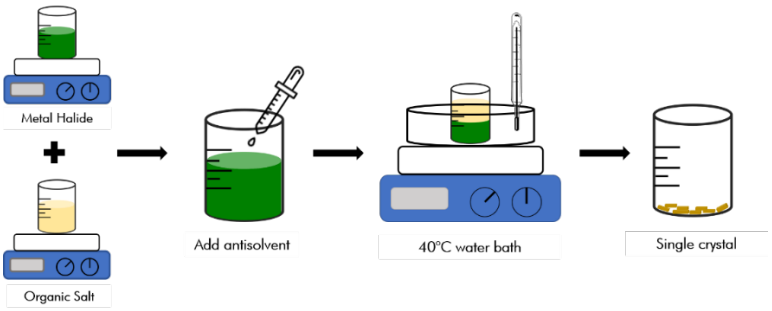

Figure 2.3 *Anti-solvent method for preparation of Cu-based layered hybrid perovskites*

Beside the slow evaporation method, various other methods to synthesize single crystals of hybrid perovskites have been reported, such as seeded solution growth, inverse temperature crystallization, and the anti-solvent method.[1] Here the anti-solvent method, also known as the layered solution growth method, was used to synthesize the copper chloride-based layered perovskite studied in chapter 5, a schematic of which is shown in Fig. 2.3. Two different solvents should be chosen that are immiscible due to different polarity. We chose methanol and acetonitrile as the solvents in this synthesis. The first step of the synthesis was identical to the method described above, where a mixture containing both the inorganic and organic components in methanol was prepared. The second solvent (acetonitrile) was added slowly to this solution until two layers had formed. The flask was placed in a 40 °C water bath, and crystals were slowly formed at the interface between the two layers. After ~3 days, all the solvent had evaporated, and the crystals remained.

2.2 Structural and Chemical Characterization

2.2.1 X-Ray Diffraction

X-ray diffraction was the main method used for structural determination in this thesis since the relatively high energy of X-rays allows them to penetrate deep into materials and provide information about the bulk structure. Powder X-ray diffraction is perhaps the most widely used technique for characterizing the structure of materials. An ideal powder sample consists of randomly oriented crystalline domains, which we attempted to obtain by grinding either ingots or

crystals using a mortar and pestle until a fine powder was obtained. However, for most of the layered materials studied in this thesis it is almost impossible to obtain random orientations of the powder grains. This is because the plate-like morphology of larger crystals is retained on grinding, leading to preferential orientation of the grains and hence biased peak intensities which makes it challenging to extract accurate structural parameters other than the unit cell dimensions. Therefore, detailed structure determinations, including determinations of bond lengths, bond angles and site-ordering, were performed using single-crystal X-ray diffraction (SC-XRD), some practical aspects of which are discussed below.

We carried out extensive SC-XRD measurements using a Bruker Venture four-circle diffractometer on single crystals of layered hybrid perovskites. The crystals were mounted either in a droplet of cryo-oil in a nylon loop for low-temperature measurements, or by fixing to a thin glass fibre using epoxy for measurements at room temperature and above where cryo-oil is less viscous and there is a risk that the crystal can move during measurement. The main requirement is to choose a high-quality single crystal of dimensions smaller than the X-ray beam (diameter ~300 μm). We used a polarized optical microscope while choosing the crystals, which has the advantage for layered materials that single crystals with a single layer orientation appear different under polarized light to polycrystals with multiple layer orientations, which often appear as single crystals with respect to their morphology under non-polarized light. The latter often show a "rainbow" effect on the crystal surface under the polarized microscope. We also avoided cutting large crystals into smaller pieces since the mechanical stress can slightly shift or rotate the weakly bound layers, resulting in smeared spots which are not favourable for structure determination.

Even when the above precautions are taken, layered crystals can often exhibit smeared spots from slight rotations of the layers, short-range order, and crystal twinning. Beside choosing a "nice" looking crystal under the microscope (a small crystal with well-defined faces, uniform colour or transparency, regular geometry, etc.), a short scan is always necessary to check the crystal quality before a more extensive measurement is started.

Crystal Twinning

Twinning was found in most of the crystals studied in this thesis. Twinning can be thought of as an intergrown crystal in which different domains are related in a symmetrical manner and share all/certain crystal lattice points. Twin domains can be associated with each other by a twin law, expressing the symmetry operation that transforms the domains into each other. Twin laws can be reflection, inversion, and rotation operations. Crystal twinning often leads to confusion during structure determination, especially when assigning a space group from so-called precession images (planes of diffracted intensity in reciprocal space). Twinning often causes reflections to appear in these images that should be forbidden by symmetry, especially in the common case of pseudo-merohedral twinning where the diffraction patterns of different domains partially overlap such that particular spots are allowed in one domain but not in the other(s) due to the crystal symmetry. For a twinned crystal, it is also common for the analysis software to assign the wrong space group based on the observed intensity distributions and apparent systematic absences. In such cases it is strongly advisable to measure a full sphere of reciprocal space in order to measure all reflections from all domains.

Generally, twinned crystals are divided into the following three types.

1. Non-merohedral twins

   Non-merohedral twins have two or more domains with reciprocal lattices that only partially overlap or more often do not overlap at all. This type of twinning leads to difficulties in the initial indexing of diffraction patterns and can be recognized by obvious multiple reciprocal lattices. However, this can only be envisaged if the reflections of one of the twin domains can be indexed. The twin operator that relates the different domains is not a symmetry element that belongs to the Laue group of the crystal itself. If only one domain gives the main contribution to the diffraction pattern and there is negligible overlap of reciprocal lattices, it is possible to solve the structure as if the crystal is single.

2. Merohedral twins

   In merohedral twins, the diffraction patterns of different domains overlap fully. The symmetry operation relating the domains is usually not part of the space group symmetry but belongs to the Laue group of the structure. During the structure determination, the crystal will appear as a single domain due to the reciprocal lattices of different domains coinciding with one another. One common type of merohedral twinning only occurs in non-centrosymmetric space groups, which is inversion twinning. This type of twinning

was often found in the work described in this thesis and should always be examined whenever a centre of symmetry is absent. In general, inversion twinning can be identified during structure refinement, for example in the SHELXL program by using the Flack test.[2] The Flack value of a non-centrosymmetric crystal with a single domain should be close to zero, whereas for inversion twinning with equal domain populations it is usually ~0.5. Inversion twinning is also known as racemic twinning in the case of chiral structures. The inversion matrix (twin law) is [-1 0 0 0 -1 0 0 0 -1].

3. Pseudo-merohedral twins

Similar to merohedral twinning, here the diffraction patterns are also fully overlapped within the resolution of the instrument. The difference is that for pseudo-merohedral twinning the symmetry operation that relates different domains is not part of the Laue group. The diffraction pattern can again be indexed using a single lattice. However, difficulties will arise during structure refinement. Inspection of reciprocal lattice planes may suggest higher Laue symmetry than the real symmetry. The diffraction data often have symmetry-allowed reflections from one domain that are superimposed at the positions of systematically absent reflections of another domain. This is often the most difficult type of twinning to recognize and analyse.

There are several issues that become apparent during various stages of data treatment, structure solution and refinement that can be used as indicators of twinning:

- Using so-called E-statistics on the reflection intensities,[3] the mean value of $|E^2-1|$ is much lower than 0.736, which is the value expected for a non-centrosymmetric crystal (centrosymmetric crystals have an expected $|E^2-1|$ of 0.968).
- The data exhibit unusual systematic absences that in some cases are not consistent with any space group.
- The structure is not solvable or when solved gives an unexpectedly poor fit to the measured intensities.
- The structural model is obtained in a centrosymmetric group but is highly distorted.
- The unit cell appears to have one or more unusually long axes, and many of the data are weak or absent.
- Some reflections are sharp, whereas others appear to be split.

Some types of crystal twinning can be modelled in the SHELX refinement program using both TWIN and BASF instructions. The twin law(s) can be defined using the TWIN instruction followed by the matrix that relates the domains. The BASF instruction is followed by one or more variable parameters that correspond to the volume fraction of each twin domain.

2.2.2 Scanning Electron Microscopy (SEM) and Energy Dispersive X-Ray Spectroscopy (EDS)

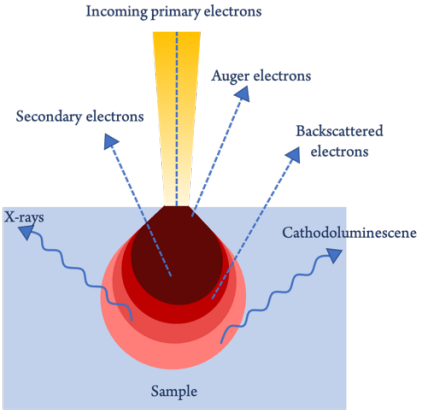

Figure 2.4 *Electron-sample interactions involved in SEM measurements.*

Scanning electron microscopy (SEM) is based on the principle that the primary electrons accelerated by the source can be scattered both elastically and inelastically by the electrons in the sample. The type of scattering and the interaction volume depends on the atomic number and electron density of the analyzed sample and the incoming electron energy (accelerating voltage). In consequence, a variety of signals will be emitted from the sample, such as secondary electrons (SEs), back-scattered electrons (BSEs), X-ray photons (which can be used for elemental analysis), and visible light, as shown in Fig. 2.4. These scattered electrons/X-rays reveal information about the sample, including surface morphology and topography, size and size distribution of different phases or grains, the height, lateral dimensions, and crystallographic orientation of nano-sized entities, as well as the chemical composition of different phases on the nano- and micro-scale.

The SEs and BSEs are mainly used for image creation in SEM. SEs provide information about the sample morphology and topography with relatively high spatial resolution since they originate from a small sample volume close to the surface. The energy of the BSEs depends on the electron density of the atoms from which they are scattered. Since BSEs are much more energetic than SEs, the signal is obtained from a greater depth (and volume) in the sample. The BSE signal thus allows visualization of electron density distribution, with brighter contrast for atoms with higher atomic numbers. This is useful for rapid phase discrimination in multiphase samples.

SEM is also widely used for elemental analysis. Characteristic X-rays are produced due to the production of photoelectrons whenever the primary electron beam is of sufficient energy to ionize atoms present in the sample. The resulting hole in the core level of the sample atom is filled by the relaxation of an electron from a higher energy level, with resulting emission of an X-ray photon, the energy of which is characteristic of that particular element. The detector records the relative intensity of the emitted X-rays versus their energy. This process, known as energy dispersive X-ray spectroscopy (EDS), is thus a chemical microanalysis technique. The EDS data can be analyzed either qualitatively or quantitatively. Qualitative analysis compares the recorded X-ray energies to the known characteristic X-ray energies of elements present in the sample. In quantitative analysis, the relative X-ray intensities are used to obtain the chemical composition of elements in the sample. A semi-quantitative analysis is most often used, without the need for analysis of any standard compounds. Mathematical corrections based on analysis parameters and sample composition are used in this technique. These analysis parameters consist of counting statistics and the choice of conditions, such as the accelerating voltage and beam current. Greater accuracy in the chemical composition can be obtained using known standards with similar structure and composition to the sample. In addition, the X-rays emitted from the sample can also be used for qualitative elemental mapping. The sample's surface is scanned, and intensity maps can be recorded for each element in the sample.

The basic requirement for SEM is to operate under vacuum conditions to avoid interaction of the electron beam with gas molecules. Moreover, to obtain high resolution, SEM samples must be electrically conductive to prevent overcharging on the surface. Overcharging may introduce extreme brightness and thus images with poor contrast.

In this thesis, SEM was used to study the microstructure of $(GeSe)_{1-x}(AgBiTe_2)_x$ alloys in chapter 3. A small piece of the synthesized ingot was inserted inside a bakelite mold of thickness ~30mm. The mold was then polished several times to expose the microstructure of the sample inside. We used a Struers polishing machine for automated polishing steps. Different sizes of graphite particles ranging from 9 to 1 μm were used for polishing. After each polishing step, the ingot was checked under an optical microscope. The last step employed a silicone-containing

solution to make the sample surface smooth. The SEM and EDS measurements were performed using a FEI Nova NanoSEM 650 with an accelerating voltage of 30kV to obtain high signal counts.

2.2.3 Differential Scanning Calorimetry (DSC)- Thermo Gravimetric Analysis (TGA)

Thermal analysis is an essential analytical tool used to study the properties of materials when heated or cooled in a controlled manner. Differential scanning calorimetry (DSC) and thermogravimetric analysis (TGA) are the most widely used thermal techniques in the characterization of crystalline and amorphous materials. Thermally-induced transitions such as phase transformations or chemical decomposition are associated with enthalpy changes. These thermal transitions are directly related to the sample structure and can involve melting, crystallization, polymorphic phase transitions, desolvation, and dehydration.

DSC records the heat flow versus the temperature of the sample and compares it to the heat flow associated with a reference sample in the same measurement setup. Heat flow to the sample can be observed as an endothermic event where heat is absorbed or an exothermic event where heat is released relative to the reference sample. DSC data are usually plotted as heat flow versus temperature and referred to as a thermogram.

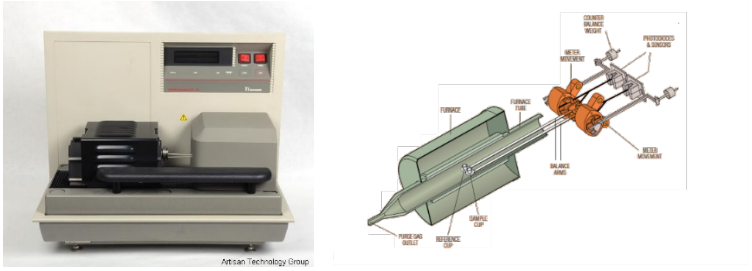

Figure 2.5 *DSC-TGA Instrument (figure adapted from TA Instruments SDT 2960 manual)*

Phase transitions between different structural polymorphs can also be associated with heat flow during DSC measurement. These transitions can be observed as either exothermic or endothermic events. However, the heat absorbed or released during polymorphic phase transitions is relatively small compared to that involved in melting or crystallization events.

TGA measures the mass change of the sample over a specific temperature range under a controlled atmosphere with a predetermined heating rate. The TGA setup consists of an electronic microbalance surrounded by a furnace. The microbalance measures changes in mass during the heating process or with respect to time at constant temperature in the case of mass loss due to thermal degradation or desolvation. DSC and TGA are usually combined (Fig. 2.5) and simultaneously measured in order to understand the thermal behaviour more thoroughly.

2.3 Thermal Transport Measurement

The thermal transport properties described in this thesis were measured using a Linseis Laser Flash Analysis (LFA) instrument, as shown in Fig. 2.6. This system consists of a xenon lamp as the laser source, a sample holder, and a detector; the components are arranged vertically.

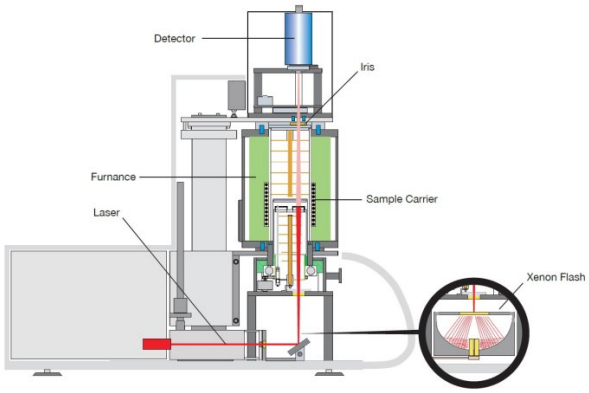

Figure 2.6 *Xenon laser flash analysis apparatus (figure adapted from Linseis XFA 600 manual)*

The thermal diffusivity of a material (usually given the symbol D or α) is related to the effective thermal inertia of a solid and determines how fast heat propagates through it. Knowing this parameter is crucial to calculate heat transfer in a solid. Thermal diffusivity measurements are widely used to determine the thermal conductivity:

$$\alpha = \frac{\kappa}{\rho \, x \, C_p} \tag{2.1}$$

Here α is the thermal diffusivity (m^2/s), κ is the thermal conductivity (W/m.K), ρ is the density of the material (kg/m^3), and C_p is the specific heat capacity (J/kg.K).

The LFA method enables rapid determination of the thermal diffusivity, specific heat capacity, and thermal conductivity of solid samples with cylindrical or rectangular geometry up to ~12 mm in their largest dimension over a range of temperatures up to 600 °C. The laser flash illuminates the bottom side of the sample, and the temperature of the upper side is measured as a function of time using an infra-red sensor.

Thin rectangular samples were prepared for the laser flash measurements on $(GeSe)_{1-x}(AgBiTe_2)_x$ alloys described in this thesis. The synthesized ingots were cut using a diamond saw to rectangular shapes and were then polished until a uniform thickness and smooth surface were achieved. In general, we prepared samples with a thickness of ~1 mm and a length ranging from 3-5 mm. Before the measurement, it is necessary to cover the surface of the sample with graphite spray, which allows the energy of the laser flash to be absorbed by the sample more uniformly.

2.4 Electrical Transport Measurement

2.4.1 High-Temperature Seebeck Coefficient and Resistivity Measurement

The Linseis LSR-3 instrument simultaneously measures the Seebeck coefficient (S) and electrical resistivity (ρ) of a bulk or thin-film material over a broad temperature range. Various sample shapes can be measured such as prismatic, square or cylindrical samples, with lengths of between 6-22mm. The sample is positioned vertically between two electrodes (see Fig. 2.7).

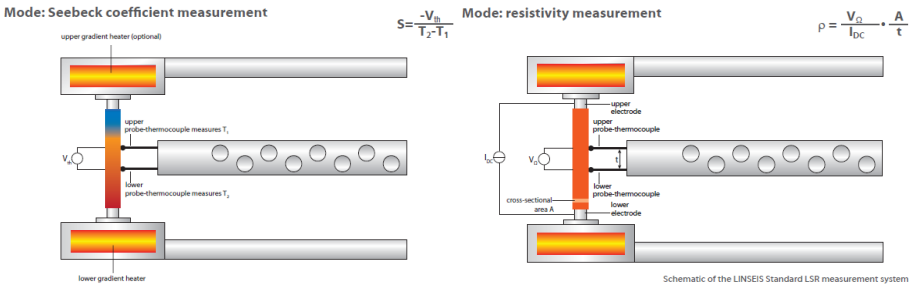

Figure 2.7 *Seebeck coefficient and electrical resistivity measurement principle (figure adapted from Linseis LSR-3 manual)*

The electrodes are located inside a furnace. In the LSR-3 instrument, the lower electrode also contains a heater that produces a temperature gradient across the sample. Two thermocouples (T_1 and T_2 in Fig. 2.7) then measure the temperature difference ($\Delta T = T_2 - T_1$) between the hot and cold sides of the sample. In addition, these thermocouples are used to measure the electromotive force dE (or thermovoltage V_{th}) that arises from the temperature gradient. From the obtained data, the Seebeck coefficient can easily be calculated:

$$S = \frac{-V_{th}}{\Delta T} \tag{2.2}$$

For determination of the electrical resistance of the sample, the dc four-terminal method is used. Here a constant current (I_{DC}) is applied through the sample between the upper and lower electrodes, and the corresponding voltage drop (V_Ω) across the sample is measured by the two thermocouples. The resistivity can be calculated when the distance between the two probes (t) and the cross-sectional sample area (A) are known, as shown in Fig. 2.7.

2.4.2 Room-Temperature Hall Effect Measurement

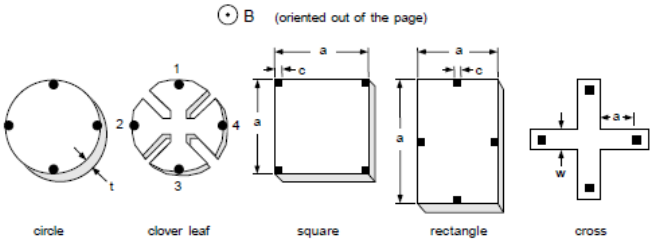

Figure. 2.8 *Possible van der Pauw sample geometries*[4]

Hall effect measurements were carried out using the four-probe technique employing the van der Pauw method. The four-probe method is known to minimize measurement errors that may arise due to the probe resistances and the contact resistances between the probe and the material. Two probes are used to apply a current, and the other two measure the voltage. The sample should have a flat surface with a uniform thickness. The sample is exposed to constant current density flow during the measurement while a magnetic field is applied. The electrical contacts between the probe and the sample should comprise a conductive material with a higher conductivity than the sample itself.

Hall effect measurements commonly use two sample geometries: a long, narrow Hall bar or nearly square or circular van der Pauw geometries. Fig. 2.8 shows common possible geometries that can be used. Compared to a Hall bar, the van der Pauw geometries are much more straightforward with respect to sample preparation for bulk materials.[5] The van der Pauw method can be used to obtain the electrical resistivity, carrier concentration, and mobility of a flat sample. [6]

In the basic van der Pauw contact arrangement, the four contacts made to the sample are numbered counter-clockwise in ascending order. In his thesis rectangular samples were used as shown in Fig. 2.8, and the the Hall coefficient can be obtained as:

$$R_{HC} = \frac{t[m]}{B[T]} \frac{V^{+}_{31,42}(+B) - V^{-}_{31,42}(+B) + V^{-}_{31,42}(-B) - V^{-}_{31,42}(-B)}{I^{+}_{31}(+B) - I^{-}_{31}(+B) + I^{-}_{31}(-B) - I^{-}_{31}(-B)} \; [m^3 \, . \, C^{-1}] \qquad (2.3)$$

and

$$R_{HD} = \frac{t[m]}{B[T]} \frac{V^{+}_{42,13}(+B) - V^{-}_{42,13}(+B) + V^{-}_{42,13}(-B) - V^{-}_{42,13}(-B)}{I^{+}_{42}(+B) - I^{-}_{42}(+B) + I^{-}_{42}(-B) - I^{-}_{42}(-B)} \; [m^3 \, . \, C^{-1}] \qquad (2.4)$$

These two values should agree within ± 10% difference. If they do not, the sample is too inhomogeneous, anisotropic, or has some other problem. If the agreement is good, then the average Hall coefficient can be calculated by:

$$R_{Hav} = \frac{R_{HC} + R_{HD}}{2} \; [m^3 . C^{-1}, cm^3 . C^{-1}] \qquad (2.5)$$

The measurement system that we used to obtain the Hall coefficient (carrier concentration) is shown in Fig. 2.9. It consists of three different pieces of equipment: a Keithley instrument as the current source, an Agilent instrument to measure the voltage, and an HP switch box. The measurements were automated using a PPMS system.

To perform a successful Hall measurement, a sample with one of the geometries allowed for the van der Pauw technique should be prepared. We used square samples with a uniform thickness of ~1 mm. It is essential to make good electrical contacts, which should be as small as possible compared to the sample size to avoid a large contact resistance, and placed at the edges of the square. Here the sample was connected to the instrument by gold wires, with contacts comprised of silver paste. Since the van der Pauw method is a 4-probe measurement, the four contacts should have similar distances, and be of approximately the same size to obtain reliable results. Each individual contact resistance was checked using a voltmeter. The resistance should be as small as possible. We performed measurements using different applied magnetic fields and found that the most reliable data were obtained with the maximum possible field of 9 T. The reliability of the data can be confirmed by comparing the voltage generated between different pairs of contacts, the magnitude of which should be similar for each pair.

Figure 2.9 *Hall coefficient measurement system and PPMS instrument (PPMS figure adapted from QD PPMS Manual)*

2.5 Magnetic Measurement

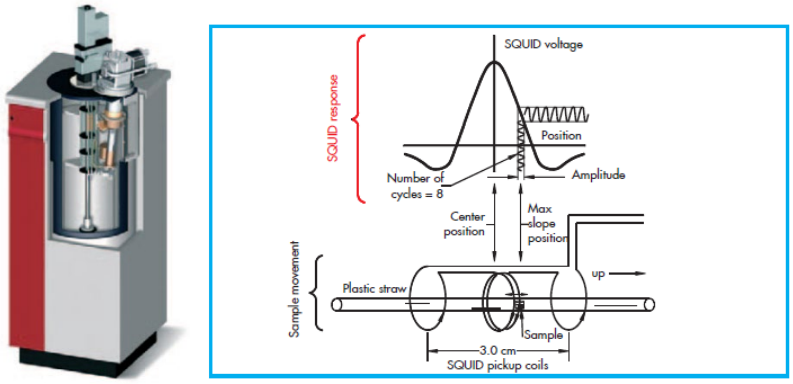

Figure 2.10 *Sample chamber of MPMS instrument and RSO mode for magnetic measurement (MPMS figure adapted from QD MPMS Manual)*

A Quantum Design Magnetic Properties Measurement System (MPMS) equipped with a Superconducting Quantum Interference Device (SQUID) was used for the magnetic measurements carried out in this thesis, as shown in Fig. 2.10. SQUID magnetometry is one of the most effective and sensitive ways of measuring magnetic properties.

During the measurement, the sample moves through superconducting detection coils generating a current flow. The SQUID then converts the current flowing in the coils to an output voltage. In a fully calibrated system, measurement of the voltage variation from the SQUID detector provides a highly accurate measurement of the sample's magnetic moment.

We used the so-called reciprocating sample option (RSO) mode to measure the magnetic properties. In the RSO mode measurements are performed using a gradiometer which moves the sample with a small amplitude and periodic displacement. The sample movement results in an oscillating AC signal detected by SQUID detector. This mode allows a high sensitivity with a minimum magnetic signal of 10^{-8} emu.

Both DC and AC magnetic measurements are possible in the MPMS. DC measurements involve the application of a DC magnetic field to determine the equilibrium value of the sample magnetization. In AC measurements, a small AC drive magnetic field is superimposed on a

constant DC field, resulting in a time-dependent moment in the sample.[7,8] At very low frequencies of AC field, this becomes similar to a DC measurement. However, at higher frequencies, the AC moment gives rise to dynamic effects. The sample magnetization during an AC measurement may lag behind the driving field, resulting in two signals recorded by the device, the magnitude of the magnetization and the phase shift. Alternatively, the magnetization can be split into an in-phase or real component M' and an out-of-phase or imaginary component, M". At low frequency, the real component can be considered as the slope of the magnetization curve, while the imaginary component is associated with dissipative processes in the sample. Both the real and imaginary components are very sensitive to the thermodynamics of phase changes and are often used to determine transition temperatures.

2.6 References

1 Y. Dang, D. Ju, L. Wang and X. Tao, *CrystEngComm*, 2016, **18**, 4476–4484.

2 G. M. Sheldrick, *Acta Crystallogr. A*, 2008, **64**, 112–122.

3 M. R. Snow and E. R. T. Tiekink, *Acta Crystallogr. B*, 1988, **44**, 676–677.

4 Lake Shore *7500/9500 Series Hall System User's Manual*, pp. 1–18.

5 K. A. Borup, E. S. Toberer, L. D. Zoltan, G. Nakatsukasa, M. Errico, J.-P. Fleurial, B. B. Iversen and G. J. Snyder, *Rev. Sci. Instrum.*, 2012, **83**, 123902.

6 R. Green, *Keithley White Paper*, 2011, pp. 1–12.

7 M. Bałanda, *Acta Phys. Pol. A*, 2013, **124**, 964–976.

8 D. Martien, *Introduction to AC Susceptibility, Quantum Design*, 1994, pp. 1-4.